Int. J. Electrochem. Sci., 14 **(2019)** 11419 – 11428, doi: 10.20964/2019.12.36

International Journal of ELECTROCHEMICAL SCIENCE
www.electrochemsci.org

Short Communication

Corrosion Inhibition Effect of a New Quinoline Derivative on Q235 Steel in H_2SO_4 Solution

Shujun Chen[1,*], *Siyi Chen*[1], *Wenpo Li*[2]

[1] School of Chemistry and Chemical Engineering, Zunyi Normal University, Zunyi 563006, China.
[2] School of Chemistry and Chemical Engineering, Chongqing University, Chongqing 400044, China.
[*]E-mail: shujunchen_znu@163.com

Received: 28 July 2019 / *Accepted:* 4 September 2019 / *Published:* 29 October 2019

In this work, a new quinoline derivative namely 5-benzyl-8-propoxyquinoline (5BPQ) has been studied to inhibit the Q235 steel corrosion in sulfuric acid. The protection ability of 5BPQ was investigated by electrochemical tests, weight loss and SEM measurements. Results indicate that the target 5BPQ has strong adsorption ability on the steel surface, thus shows excellent corrosion protective performance for steel in acid solution. The maximum inhibition efficiency of 5BPQ is 97.7%), which is attributed to the effect of the heterocyclic rings. Scanning electron microscope (SEM) was utilized to further analysis the appearance of steel surface. Furthermore, the quantum calculation and molecular dynamics (MD) simulation further supported experiment. The systematic study gives a new guide to design novel quinoline derivative molecules to obtain the corrosion protection ability.

Keywords: Corrosion Inhibitor; Q235 steel; SEM; MD Simulation.

1. INTRODUCTION

Corrosion is a very serious problem and the method of introducing corrosion inhibitors in small quantities is a convenient method to prevent corrosion [1, 2]. The corrosion inhibitor can effectively protect the surface of the metal and the alloy, so that the corrosion rate in the corrosive medium is significantly reduced, thereby maintaining the excellent performance of the metal material itself. The advantages of corrosion inhibitors can be summarized as follows: simple operation, small amount, high efficiency, wide application, and high economic benefits, etc [3-5]. The most effective inhibitors are organics containing the heteroatoms (N, S, O and P) in a conjugated system, which act as active centers for their interaction with metal surface [6-9]. However, most of these compounds used towards metal corrosion in acidic media are toxic, and expensive, causing a lot of pollution to the environment. Therefore, many attempts have been carried out to find eco-friendly inhibitors for metal materials in recent years [10-15]. Qiang have developed four allyl imidazolium-based ionic liquids (ILs) with various

length of alkyl chains for the corrosion inhibition of copper in 0.5 M sulfuric acid [10]. These compounds exhibit superior inhibitive ability for copper corrosion. Tan investigated the inhibition performance of two food flavors of 2-isobutylthiazole (ITT) and 1-(1,3-Thiazol-2-yl)ethanone (TEO) for X65 steel corrosion in H_2SO_4 were studied by various methods [16]. The results of experimental and theoretical studies have shown that the inhibition effect of TEO is better than ITT.

In this work, a harmfulless quinoline derivative namely 5-benzyl-8-propoxyquinoline (5BPQ) were explored as promising corrosion inhibitors of Q235 steel in sulfuric acid, which is not reported before. For this study, the aim is to shed deep lights to inhibition mechanism of related quinoline derivatives. The inhibition performance was researched by weight loss experiment, Electrochemical impedance spectroscopy (EIS), potentiodynamic polarization, as well as scanning electron microscope (SEM). The quantum chemical calculation and molecular dynamics (MD) simulation were furtherly used to give evidence to the adsorption and inhibition mechanism.

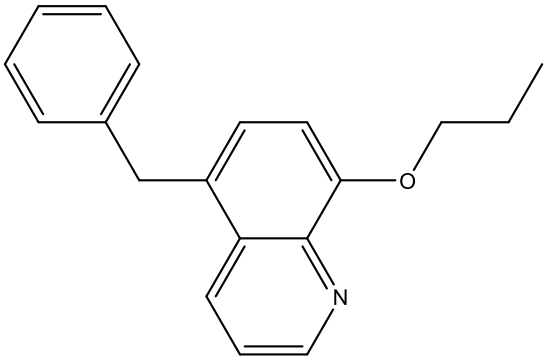

Figure 1. The molecular structure of 5BPQ.

2. EXPERIMENTAL

2.1. Materials

All the reagents were used directly without further purification and deionized water was used as solvent. 5BPQ was bought from Titan without any synthesis and purification. The 0.5 M H_2SO_4 solution were used as the blank for comparison. The test solution was 0.5 M H_2SO_4 solution with different concentrations of 5BPQ (2, 4, 6, 8 mM). And the temperature was controlled by the water bath. Q235 steel was the selected metal material. Emery papers (400, 800, 1200, 2000, and 3000 grades) were used to remove the oxide layer from the steel specimens. Then the specimens were rinsed with ethanol and deionized water, and finally dried. Finally, the samples were dried at room temperature for use.

2.2. Weight loss

Some 150 mL glass beakers were used to perform the gravimetric test. Freshly polished steel specimens were weighted and immersed in 0.5 M H_2SO_4 with different concentrations of 5BPQ for 5 h

in triplicate at 298, 308 and 318 K, respectively. After that, the steel specimens were charily withdrawn, carefully rinsed in ultrapure water and acetone, then dried and weighted. Finally, the mean corrosion rates were obtained.

2.3. Electrochemical measurements

Electrochemical tests were accomplished by a three-electrode system using electrochemical station (CHI 660E). Saturated calomel electrode (SCE), Q235 steel, and Pt sheet were utilized as the reference electrode, working electrode and the counter electrode, respectively. Open circuit potential measurement was first carried out. Then EIS was recorded at OCP in 100 kHz to 0.01 Hz frequency range with 5 mV peak AC signal. The obtained inhibition efficiencies are defined by,

$$\eta(\%) = (1 - \frac{R_{ct,0}}{R_{ct}}) \times 100 \qquad (1)$$

where $R_{ct,0}$ and R_{ct} show unprotected and protected charge transfer resistance, respectively.

Finally, the polarization curves were performed at 1 mV/s scan rate and in the range of ±250 mV of OCP. The relevant inhibition efficiency is determined as follows:

$$\eta(\%) = (1 - \frac{i_{corr}}{i_{corr,0}}) \times 100 \qquad (2)$$

where $i_{corr,0}$ and i_{corr} show unprotected and protected current densities, respectively.

2.4. SEM

In order to investigate the surface topography of steel sample with and without protection of 5BPQ, scanning electron microscope (SEM, JEOL-JSM-7800F, Japan) was applied.

2.5. Calculation details

The quantum chemical calculation (Dmol3) based on density functional theory (DFT) was used to optimize the molecular structure. The optimized frontier molecular orbital and related parameters including the energy of highest occupied molecular orbital (E_{HOMO}), the energy of lowest unoccupied molecular orbital (E_{LUMO}), the dipole moment (μ), and energy gap (ΔE) were obtained. Besides, the molecular dynamics (MD) simulation was performed by the Forcite module in order to explore the interaction between 5BPQ and Fe (110) surface. The simulation was processed using the periodic boundary conditions under COMPASS force field at NVT canonical ensemble with a time step of 1.0 fs and simulation time of 300 ps.

3. RESULTS AND DISCUSSION

3.1. Potentiodynamic polarization

Fig. 2 shows the potentiodynamic polarization curves of Q235 steel in 0.5 M H_2SO_4 solution with different concentrations of 5BPQ. Table 1 shows the. The corresponding experimental results parameters, including i_{corr} (corrosion current density), E_{corr} (corrosion potential), β_c (cathodic Tafel slope), β_a (anodic Tafel slope), were calculated and listed in Table 1. As seen that after adding 5BPQ to the corrosion system, both the cathodic polarization curve and the anodic polarization curve are significantly reduced, and the current density is rapidly reduced. All the corrosion inhibition efficiency values are higher than 90.0%, which indicates that 5BPQ has a strong inhibitory effect on the corrosion reaction of the cathode and anode.

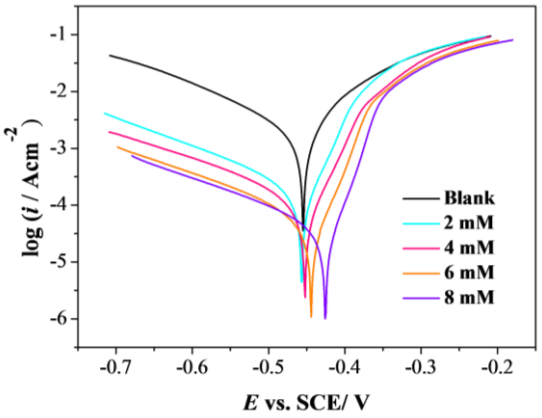

Figure 2. Polarization curves of steel with different concentrations of 5BPQ.

The cathodic polarization curves are arranged in parallel, and the slope βc does not change much, indicating that the corrosion inhibitor does not affect the cathodic corrosion reaction mechanism [17-19]. In the vicinity of the polarization potential -350 mV, the slope of the polarization curve of the anode region is significantly increased. It is believed that the adsorption-desorption equilibrium of the corrosion inhibitor on the surface of Q235 steel is destroyed at this time, so that the adsorption rate is higher that desorbed rate at this potential. The change of corrosion potential is less than 85 mV, indicating 5BPQ acts as a mixed-type corrosion inhibitor for Q235 steel [20]. Remarkably, the maximum value of inhibition efficiency is reached up to 97.7% at 8 mM, indicating the superior inhibitory ability of 5BPQ.

Table 1. Polarization parameters for Q235 steel in H_2SO_4 solution with diverse concentrations of 5BPQ

C (mM)	E_{corr} (mV)	i_{corr} (mA cm^{-2})	β_c (mV dec^{-1})	β_a (mV dec^{-1})	η (%)
0	–459	1.75	–149	111	/
2	–456	0.14	–151	113	92.0
4	–465	0.11	–150	77	93.7
6	–467	0.08	–144	46	95.4
8	–450	0.04	–157	38	97.7

3.2. EIS measurement

Fig. 3 shows the Nyquist and Bode plots of Q235 steel in 0.5 M H2SO4 solution with different concentrations of 5BPQ, and the equivalent circuit diagram of Fig. 4 is used to fit the data by ZSimpWin software. The circuit consists of solution resistance (*R*s), charge-transfer resistance (R_{ct}), constant phase element (*CPE*), and inductive elements (R_L and L). The relevant C_{dl} (double layer capacitance) can be obtained as follows [21, 22]:

$$C_{dl} = Y_0 \left(2\pi f_{max}\right)^{n-1} \quad (3)$$

where Y_0 is impedance magnitude, f_{max} is the frequency at the maximum imaginary component value, and *n* is the deviation parameter. The fitting results are shown in Table 2.

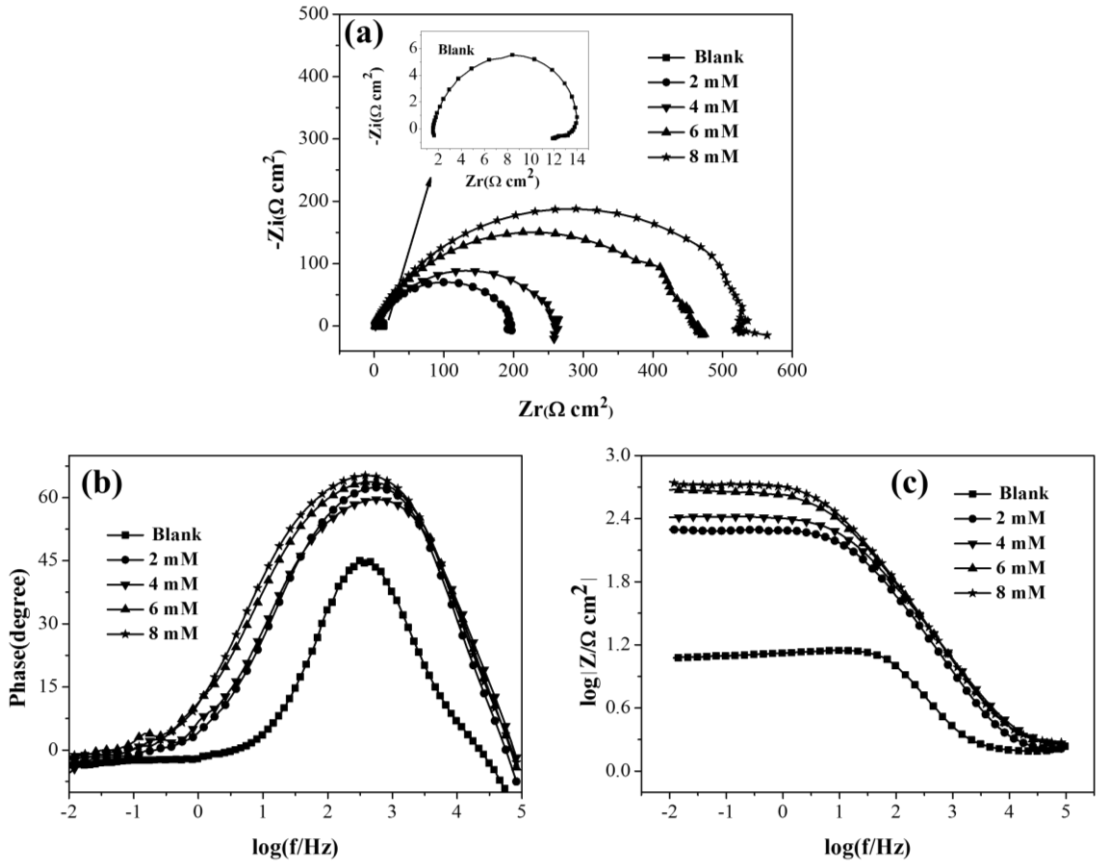

Figure 3. The Nyquist (a) and Bode (b, c) plots for steel electrode with different concentrations of 5BPQ

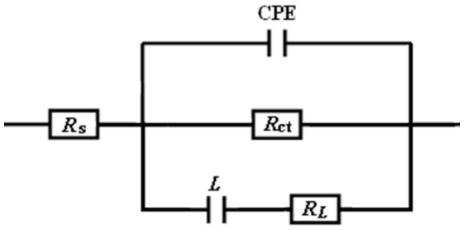

Figure 4. The used electrical circuit.

It can be seen from Fig. 3 that with the addition of 5BPQ, the radius of the capacitive arc of the system becomes larger, showing the excellent corrosion inhibition performance of 5BPQ. In addition, the shape of the impedance has not changed with various concentrations, which indicates that the increase of concentration will not change the corrosion mechanism [23]. As shown in Table 2, the concentration of corrosion inhibitor increases, R_{ct} increases, which indicates that the corrosion process becomes more difficult. The corrosion inhibition efficiency increases gradually, and the regularity is consistent with polarization results. The electric double layer capacitor C_{dl} gradually becomes smaller due to the addition of the corrosion inhibitor, which embodies that the corrosion inhibitor molecules compete with the water molecules for more adsorption on the metal surface, and the smaller dielectric constant is also the reason why the C_{dl} becomes smaller [9, 24, 25].

Table 2. EIS parameters of Q235 steel in H_2SO_4 solution with different concentrations of 5BPQ

C (mM)	C_{dl} (μF cm^{-2})	R_{ct} (Ω cm^2)	*L* (Ω cm^2)	R_L (Ω cm^2)	*η* (%)
0	125.4	13.5	20.5	65.2	/
2.0	45.1	146.1	5820	1157	90.8
4.0	46.6	262.4	3974	376	94.9
6.0	42.8	447.1	1672	0.20	97.0
8.0	41.0	529.6	844	18	97.5

From the corrosion inhibition efficiency, it can be seen that when the concentration of 5BPQ is 2 mM, the efficiency has reached 90.8%. Then, with the increase of concentration, the inhibition efficiency is continuously increased with a maximum value of 97.5%. The obtained inhibition efficiencies agree well with those calculated from polarization test, revealing the excellent corrosion resistance of 5BPQ for Q235 steel in H_2SO_4 medium.

3.3. Weight loss study

Inhibition action of 5BPQ at different temperatures on steel corrosion was investigated by weight loss and the results are shown in Fig. 5. The relevant corrosion rate (*v*) and *η* are calculated as follows.

$$v = \frac{W_0 - W}{St} \quad (4)$$

$$\eta(\%) = \frac{v_0 - v}{v_0} \times 100 \quad (5)$$

where *S* is surface area, *t* is immersion time, W_0 and *W* are the samples weight before and after exposure in corrosive solution, v_0 and *v* are the corrosion rates without and with inhibitor, respectively.

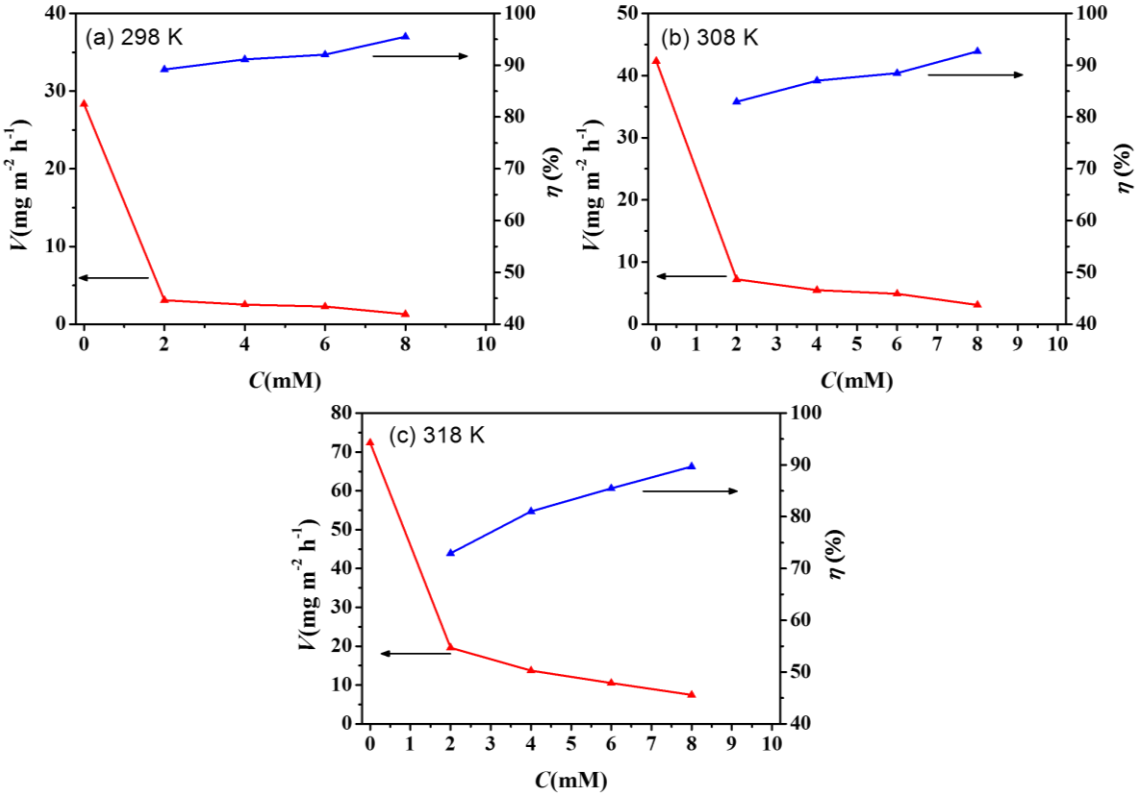

Figure 5. The weight loss graph of Q235 steel in 0.5 M H_2SO_4 without and with 5BPQ at various 298-318 K.

It can be seen from the data, at various temperatures, with the addition of 5BPQ, the corrosion rate of Q235 steel in the corrosion system is significantly reduced, and the inhibition efficiency on the corrosion reaction is further enhanced. In addition, the weight loss results are in good agreement with the previous electrochemical test results, which proves that studied compound has excellent corrosion inhibition effect on Q235 steel in H_2SO_4.

3.4. SEM observation

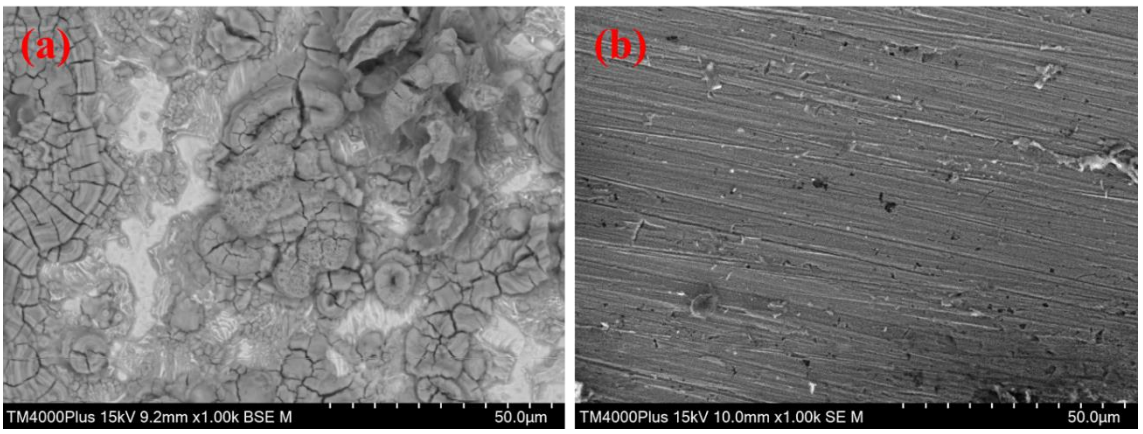

Figure 6. SEM images of steel without (a) and with (b) the protection of 8 mM 5BPQ

In order to further study the inhibition effect of 5BPQ, Fig. 6 shows SEM diagrams in absence and presence of 8 mM 5BPQ at 298 K. As seen in Fig. 6a, the steel surface is badly corroded due to the aggressive acid attack. As for Fig. 6b, steel surface become smooth relatively smooth and less damaged With the addition of 5BPQ, suggesting the great protective ability of 5BPQ for steel.

3.5. DFT calculation

The use of quantum chemistry calculation to study the relationship between the structure of corrosion inhibitor molecules and its corrosion inhibition performance can be of great help in exploring the mechanism of corrosion protection, and can also provide guidance for seeking better corrosion inhibitors in the future [26-28]. Therefore, optimized structure and molecular frontier orbital diagrams of 5BPQ are shown in Fig. 7. The related quantum chemical parameters including E_{HOMO}, E_{LUMO}, the gap energy (ΔE), the dipole moment (μ) are summarized in Table 3.

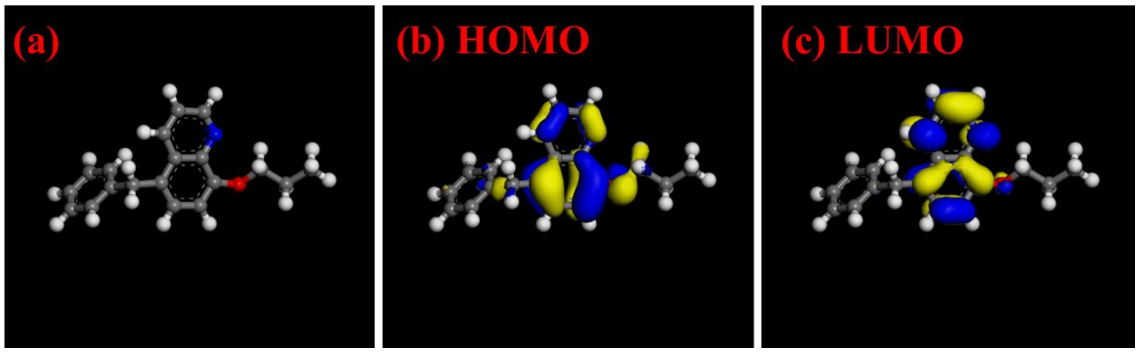

Figure 7. The molecular frontier orbital diagrams of 5BPQ.

Table 3. The quantum chemical parameters of 5BPQ.

E_{HOMO}(eV)	E_{LUMO}(eV)	ΔE(eV)	μ(D)
□8.45	□5.31	3.14	11.4

From Fig. 7, HOMO and LOMO of 5BPQ are both localized on the quinoline ring and O atom, which would act as active centres to form coordinate bonds with steel surface. According to the frontier orbital theory, the molecular reactivity of a compound is closely associated with both HOMO and LUMO. The HOMO is related to the ability of a molecule to donate electrons, and LUMO is the ability of a molecule to accept electrons [23, 29]. High E_{HOMO} value and low E_{LUMO} values mean strong reactivity of the molecule. Therefore, the lower ΔE shows greater polarization and stronger adsorption of the molecule onto metal [30]. In this study, the low ΔE for 5BPQ (Table 3) suggests great inhibition performance. In addition, the harbors a significant role to examine the inhibition ability of organic inhibitors. it can be accepted that the molecule with higher dipole moment (μ) is more likely to assemble to metal and thus showing better protective performance [31]. In present study, the high value of μ for

5BPQ is 11.4 Debye, indicating the strong adsorption of 5BPQ molecules compare to H_2O molecule, which confirms the rationalization of the experimental data.

3.6. Molecular dynamics simulation

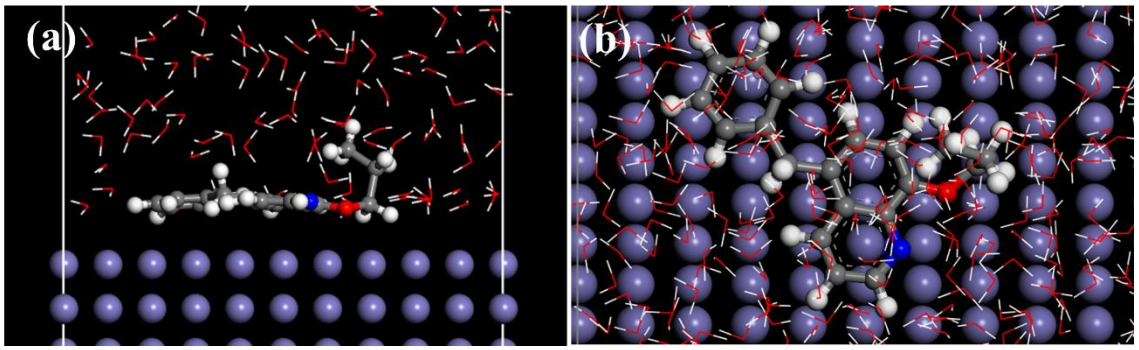

Figure 8. Side and top views of the adsorption equilibrium configurations for 5BPQ on Fe(110) surface

In order to further investigating the interaction between 5BPQ and steel, the MD simulation was performed. Fig. 8 shows the relevant side and on-top views of equilibrium configuration of 5BPQ on Fe (110) surface. As seen that the 5BPQ molecule is closely adsorbed on Fe surface with a parallel mode, where a chemical bond could occur through donation of the lone pair of the heteroatoms to the Fe. Meanwhile, an alkyl chain is vertical to the surface to form a hydrophobic film to prevent the corrosive attack. In addition, the interaction energy ($E_{interact}$) between inhibitor molecules and the steel surface were also calculated with the method in the literature [23, 32]. The obtained $E_{interact}$ is a high value of 220.8 kcal/mol, meaning that the inhibitor can adsorb onto the steel surface easily and strongly. The results confirm its superior experimental inhibition performance of 5BPQ above.

4. CONCLUSIONS

The following conclusions can be drawn:

(1) Electrochemical results show that 5BPQ is a mixed-type inhibitor with great inhibition performance for Q235 steel in 0.5 M Sulphur acid.

(2) Weight loss experiment agrees well with electrochemical results. The inhibition efficiency increases with increasing concentration and still high values at higher temperatures.

(3) SEM confirmed the inhibitive ability of 5BPQ and indicated that the adsorption film is formed on steel surface.

(4) The DFT and MD study is consistent with the experimental data and provide novel evidence for the mechanism of 5BPQ.

References

1. Y.J. Qiang, S.T. Zhang, S.Y. Xu, L.L. Yin, *RSC Adv.*, 5 (2015) 63866-63873.
2. Y. Qiang, S. Zhang, S. Xu, W. Li, *J. Colloid Interf. Sci*., 472 (2016) 52-59.
3. Z. Salarvand, M. Amirnasr, M. Talebian, K. Raeissi, S. Meghdadi, *Corros. Sci*. 114 (2017) 133-145.
4. G. Sığırcık, D. Yildirim, T. Tüken, *Corros. Sci.* 120 (2017) 184-193.
5. Z. Gong, *Inter. J. Electrochem. Sci.,* (2018) 8072-8083.
6. Y. Qiang, S. Zhang, S. Xu, L. Guo, N. Chen, I.B. Obot, *Inter. J. Electrochem. Sci*., 11 (2016) 3147-3163.
7. P. Mourya, P. Singh, R.B. Rastogi, M.M. Singh, *Appl. Surf. Sci.*, 380 (2016) 141-150.
8. Y. Wang, Y. Zuo, X. Zhao, S. Zha, *Appl. Surf. Sci.*, 379 (2016) 98-110.
9. Y. Qiang, S. Zhang, L. Guo, S. Xu, L. Feng, I.B. Obot, S. Chen, *J. Clean. Prod.*, 152 (2017) 17-25.
10. Y. Qiang, S. Zhang, L. Guo, X. Zheng, B. Xiang, S. Chen, *Corros. Sci*., 119 (2017) 68-78.
11. Y. Qiang, S. Zhang, B. Tan, S. Chen, *Corros. Sci.*, 133 (2018) 6-16.
12. B. Tan, S. Zhang, H. Liu, Y. Qiang, W. Li, L. Guo, S. Chen, *J. Taiwan Inst. Chem. E.*, 102 (2019) 424-437.
13. Y. Yu, D. Zhang, H. Zeng, B. Xie, L. Gao, T. Lin, *Appl. Surf. Sci*., 355 (2015) 1229-1237.
14. Ž.Z. Tasić, M.B. Petrović Mihajlović, M.B. Radovanović, M.M. Antonijević, *J. Mol. Liq.*, 265 (2018) 687-692.
15. Y. Qiang, S. Zhang, H. Zhao, B. Tan, L. Wang, *Corr. Sci.*, (2019) https://doi.org/10.1016/j.corsci.2019.108193 avialable online.
16. B. Tan, S. Zhang, H. Liu, Y. Guo, Y. Qiang, W. Li, L. Guo, C. Xu, S. Chen, *J. Colloid Interf. Sci*., 538 (2019) 519-529.
17. P. Kannan, T.S. Rao, N. Rajendran, *J. Colloid Interf. Sci.*, 512 (2018) 618-628.
18. M. Prabakaran, S.-H. Kim, N. Mugila, V. Hemapriya, K. Parameswari, S. Chitra, I.-M. Chung, *J. Ind. Eng. Chem.*, 52 (2017) 235-242.
19. P.E. Alvarez, M.V. Fiori-Bimbi, A. Neske, S.A. Brandán, C.A. Gervasi, *J. Ind. Eng. Chem.*, 58 (2018) 92-99.
20. Y. Qiang, S. Fu, S. Zhang, S. Chen, X. Zou, *Corros. Sci*., 140 (2018) 111-121.
21. Z. Ghelichkhah, S. Sharifi-Asl, K. Farhadi, S. Banisaied, S. Ahmadi, D.D. Macdonald, *Corros. Sci.*, 91 (2015) 129-139.
22. Y. Gong, Z. Wang, F. Gao, S. Zhang, H. Li, *Ind. Eng. Chem. Res.*, 54 (2015) 12242-12253.
23. Y. Qiang, S. Zhang, L. Wang, *Appl. Surf. Sci*., 492 (2019) 228-238.
24. H. Lgaz, R. Salghi, K. Subrahmanya Bhat, A. Chaouiki, Shubhalaxmi, S. Jodeh, *J. Mol. Liq.*, 244 (2017) 154-168.
25. M.B.P. Mihajlovic, M.B. Radovanovic, Z.Z. Tasic, M.M. Antonijevic, *J. Mol. Liq.*, 225 (2017) 127-136.
26. Z. Hu, Y. Meng, X. Ma, H. Zhu, J. Li, C. Li, D. Cao, *Corros. Sci.*, 112 (2016) 563-575.
27. P. Singh, E.E. Ebenso, L.O. Olasunkanmi, I.B. Obot, M.A. Quraishi, *J. Phys. Chem*. C, 120 (2016) 3408-3419.
28. D. Zhang, Y. Tang, S. Qi, D. Dong, H. Cang, G. Lu, *Corros. Sci*., 102 (2016) 517-522.
29. Y. Qiang, S. Zhang, Q. Xiang, B. Tan, W. Li, S. Chen, L. Guo, *RSC Adv.*, 8 (2018) 38860-38871.
30. A. Singh, K.R. Ansari, M.A. Quraishi, H. Lgaz, Y. Lin, *J. Alloy Compd*., 762 (2018) 347-362.
31. Y. Qiang, S. Zhang, S. Yan, X. Zou, S. Chen, *Corros. Sci*., 126 (2017) 295-304.
32. B. Tan, S. Zhang, Y. Qiang, L. Feng, C. Liao, Y. Xu, S. Chen, *J. Mol. Liq*., 248 (2017) 902-910.